Synthesis of Two-Dimensional Nb1.33C (MXene) with Randomly Distributed Vacancies by Etching of the Quaternary Solid Solution (Nb2/3Sc1/3)2AlC MAX Phase

Joseph Halim, Justinas Palisaitis, Jun Lu, Jimmy Thörnberg, Moon E. J., Precner M., Per Eklund, Per O. Å. Persson, Barsoum M. W. and Johanna Rosén

Halim, J., Palisaitis, J., Lu, J., Thörnberg, J., E. J., M., M., P., Eklund, P., Persson, P. O. Å., M. W., B., Rosén, J., (2018), Synthesis of Two-Dimensional Nb1.33C (MXene) with Randomly Distributed Vacancies by Etching of the Quaternary Solid Solution (Nb2/3Sc1/3)2AlC MAX Phase, *ACS Applied Nano Materials*, 1(6), 2455-2460. https://doi.org/10.1021/acsanm.8b00332

Original publication available at:
https://doi.org/10.1021/acsanm.8b00332

Synthesis of two-dimensional $Nb_{1.33}C$ (MXene) with randomly distributed vacancies by etching of the quaternary solid solution $(Nb_{2/3}Sc_{1/3})_2AlC$ MAX phase

*J. Halim,[a] J. Palisaitis,[a] J. Lu,[a] J. Thörnberg,[a] E.J. Moon,[b] M. Precner,[c] P. Eklund, P. O. Å. Persson,[a] M. W. Barsoum,[b] and J. Rosen[a,]**

AUTHOR ADDRESS

[a] Thin Film Physics, Department of Physics, Chemistry, and Biology (IFM), Linkoping, Sweden

[b] Department of Materials Science and Engineering, Drexel University, PA 19104, USA

[c] Institute of Electrical Engineering, Slovak Academy of Sciences, 84104 Bratislava, Slovak Republic

KEYWORDS

Transition metal carbide; 2D material; synthesis; MXene; electronic properties

ABSTRACT

Introducing point defects in two dimensional, 2D, materials can alter or enhance their properties. Here, we demonstrate how etching a laminated $(Nb_{2/3}Sc_{1/3})_2AlC$ MAX phase (solid solution) of both the Sc and Al atoms, results in a 2D $Nb_{1.33}C$ material (MXene) with a large number of vacancies and vacancy clusters. This method is applicable to any quaternary, or higher, MAX phase wherein one of the transition metals is more reactive than the other and could be of vital importance in applications such as catalysis and energy storage. We also report, for the first time, on the existence of $(Nb_{2/3}Sc_{1/3})_3AlC_2$ and $(Nb_{2/3}Sc_{1/3})_4AlC_3$ phases.

Two-dimensional (2D) materials have shown great promise for many applications.[1-6] The reduced dimension leads to an increase in the surface to volume ratio, and can fundamentally alter the chemical, optical and electronic properties of a material. The properties can be altered further, either chemically via surface functionalization,[7] intercalation[8] or structurally, by introducing defects.[8-9]

About 7 years ago, a new class of 2D materials based on transition metal carbides and/or nitrides (MXenes) was discovered.[10-11] MXenes are mainly produced by etching the $M_{n+1}AX_n$ (MAX) phases or related ternary phases.[12] The MAX phases are a family of hexagonal, layered ternary transition metal carbides and/or nitrides where M stands for an early transition metal, A stands for group 13 and 14 elements, X stands for carbon and/or nitrogen and n = 1, 2, or 3.[13] Various acidic solutions, containing fluoride ions are used to selectively etch the A layers (either Al or Ga) and convert MAX to MXene.[10, 14-17] The A layers are replaced with oxygen, hydroxyl and/or fluoride surface terminating (T) groups.[18] MXenes show promise for a large host of applications including batteries, supercapacitors, transparent conducting electrodes, catalytic and photocatalytic applications, water treatment, electromagnetic shielding, gas sensors and biosensors.[19-25]

MXene properties can be tuned in at least three ways that involve either altering their: i) composition, ii) surface terminations, T_x and/or, iii) structure/morphology. The composition can be changed by e.g. forming solid solutions though alloying on the M-,[26] and/or X-[27] sites in the parent MAX phase. The quaternaries, $(Nb_{0.8},Ti_{0.2})_4C_3T_x$ and $(Nb_{0.8},Zr_{0.2})_4C_3T_x$[28] are examples

in which M-site MAX solid solution phases were etched to produce their MXenes. Ti_3CNT_x is an example of a MXene with X-site solid solution.[11] Altering the surface terminations can be made by chemical treatment such as alkali treatment and/or post-etching heat treatment to remove F terminations.[29-30]

Quite recently quaternary n = 1, or 211, MAX phases with in-plane chemical ordering were discovered. These phases were labeled *i*-MAX because of the ordering of two different M elements, in a 2:1 ratio, in the basal planes. The first example was $(Mo_{2/3}Sc_{1/3})_2AlC$.[31] When this phase was etched both the Al and Sc atoms were removed and a MXene - $Mo_{1.33}CT_z$ wherein the vacancies were ordered - was produced. This vacancy-ordered 2D material exhibited a three orders of magnitude higher electrical conductivity and a 65% higher capacitance when used as a supercapacitor electrode compared to Mo_2CT_x. Furthermore, an ultrathin flexible $Mo_{1.33}CT_x$/polymer film showed promising performance as a solid-state supercapacitor.[32] Since then, other *i*-MAX phases have been theoretically predicted and synthesized such as $(V_{2/3}Zr_{1/3})_2AlC$, $(Mo_{2/3}Y_{1/3})_2AlC$ and $(Cr_{2/3}Sc_{1/3})_2AlC$.[33-34] A characteristic feature of the *i*-MAX phases is that the minority M elements extends from the M towards the Al layers, with a structure described by a (*C2/c)* or (*C2/m*) symmetry.[32] This is opposed to the traditional MAX phase of $P6_3/mmc$ symmetry, which describes most quaternary 211 MAX phases (solid solutions) realized.

A large majority of MXene work to date has been carried out on $Ti_3C_2T_x$. There are others, however. Recently, Nb_2CT_x flakes have shown promising performance for photothermal cell ablation and as a photocatalyst for hydrogen evolution in addition to previously reported results for energy storage applications.[35-38] These reports were the impetus for this work, together with our recent discovery of a quaternary *i*-MAX phase in which the minority M element – Sc in this case – was readily etched.

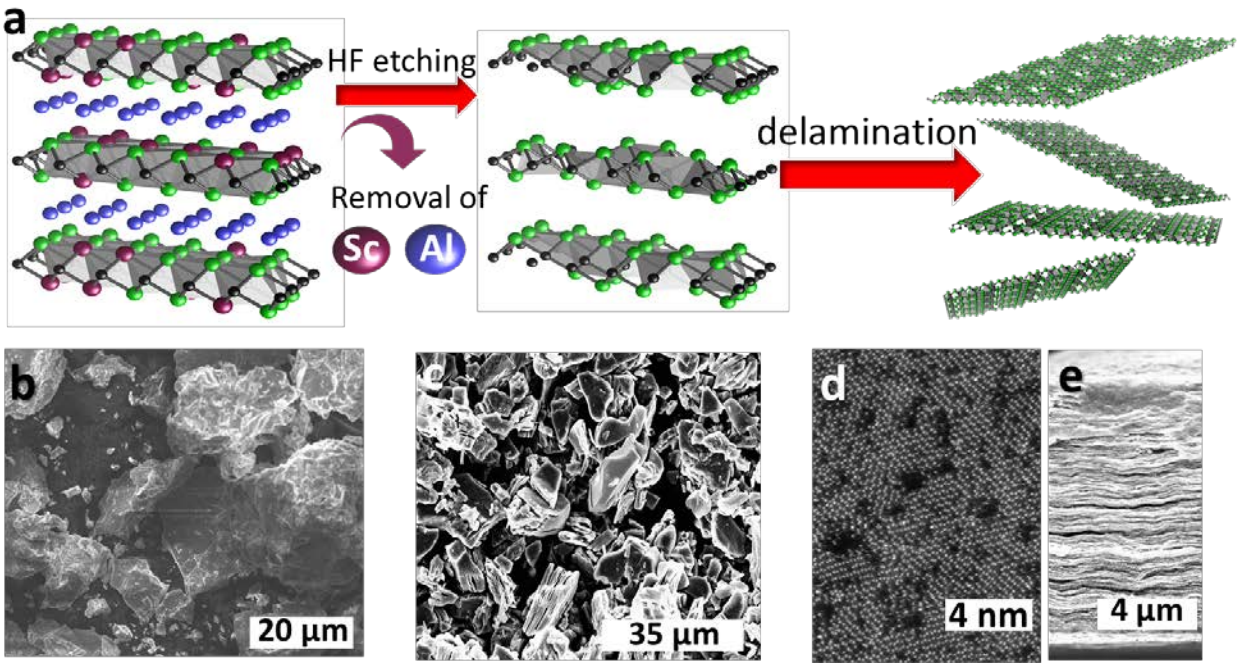

Figure 1. (a) Schematic showing synthesis, etching and delamination of $(Nb_{2/3}Sc_{1/3})_2AlC$ to form $Nb_{1.33}CT_x$. Green, black, red and blue atoms represent Nb, C, Sc, and Al, respectively, (b) SEM micrograph of $(Nb_{2/3}Sc_{1/3})_2AlC$ powders, (c) SEM micrograph of multi-layered $Nb_{1.33}CT_x$ powders, and (d) STEM micrograph of a single $Nb_{1.33}CT_x$ flake and (e) SEM micrograph of cross-section of free-standing film made from delaminated *d*-$Nb_{1.33}CT_x$.

First, we synthesized the new quaternary MAX solid solution, $(Nb_{2/3}Sc_{1/3})_2AlC$, wherein the M elements Nb and Sc are not ordered. We then selectively etched both Al and Sc atoms to produce $Nb_{1.33}CT_x$, with randomly distributed vacancies and vacancy clusters. A schematic of our approach is shown in Figure 1a. In principle this method should be applicable to any quaternary MAX phase in which the minority M-element is etchable.

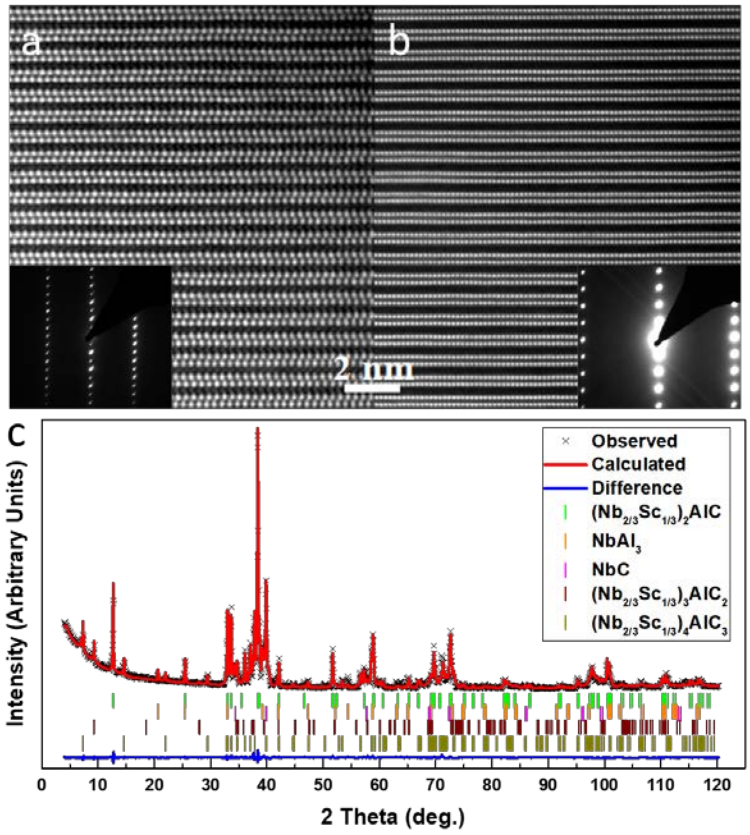

Figure 2. (a) STEM micrograph with SAED of $(Nb_{2/3}Sc_{1/3})_2AlC$ in $[11\bar{2}0]$ zone axis, b) same as a but in $[10\bar{1}0]$ zone axes, and (c) XRD patterns indexed to $(Nb_{2/3}Sc_{1/3})_2AlC$ powder showing observed pattern (black crosses), Rietveld generated pattern (red line) and the difference between the two (blue line). The green, orange, purple, violet and olive ticks below the pattern represent the peak positions of $(Nb_{2/3}Sc_{1/3})_2AlC$, $NbAl_3$, NbC, $(Nb_{2/3}Sc_{1/3})_3AlC_2$, and $(Nb_{2/3}Sc_{1/3})_4AlC_3$ phases, respectively.

The quaternary solid solution, $(Nb_{2/3}Sc_{1/3})_2AlC$, was synthetized by reacting the elemental powders, Nb, Sc, Al, and, C in a molar ratio of 4/3:2/3:1:1 at 1400 ˚C for 2 h in flowing Ar (processing details can be found in Supporting Information). The crystal structure is shown in leftmost panel in Figure 1a. Figures 1b and 1c show Scanning Electron Microscope, SEM, images of the $(Nb_{2/3}Sc_{1/3})_2AlC$ powders before, and after, etching, respectively. Figure 1d shows a typical

Scanning Transmission Electron Microscope, STEM, image of a single $Nb_{1.33}CT_x$ flake showing vacancies and vacancy clusters. The removal of Sc atoms was confirmed by electron energy loss spectroscopy analysis (see Supplementary Information, Figure S1). Figure 1e shows a cross-sectional SEM image of a free standing thin film made by filtering delaminated $Nb_{1.33}CT_x$ flakes.

The STEM images, shown in Figure 2,a and b, show the typical MAX phase layered structure.[13] The MAX phase identification is further confirmed by the selected area electron diffraction, SAED, (inset in Figure 2a,b). Rietveld refinement analysis of a powder the X-ray diffraction (XRD) pattern (Figure 2c) was used to quantify the various phases present. According to Rietveld analysis (refinement details can be found in the Supplementary Information), the sample contained the following phases: $(Nb_{2/3}Sc_{1/3})_2AlC$, $NbAl_3$, NbC, $(Nb_{2/3}Sc_{1/3})_3AlC_2$, and $(Nb_{2/3}Sc_{1/3})_4AlC_3$ with weight % of: 68(2) wt.%, 10.1(4) wt.%, 17.4(4) wt.%, 2.5(3) wt.%, and 2.0(2) wt.%, respectively. When all the phases were considered, the χ^2 value was 8.78. Note that the powder showed evidence for $(Nb_{2/3}Sc_{1/3})_{n+1}AlC_n$, with n = 1, 2 and 3.

For the main phase $(Nb_{2/3}Sc_{1/3})_2AlC$, since Nb and Sc are randomly distributed in transition metal position, the quaternary MAX phase retains the *P6$_3$/mmc* symmetry of ternary MAX phases. The *a* and *c* lattice parameters were calculated to be 3.12915(5) Å and 13.9736(3) Å, respectively, which agree with those obtained from STEM and SAED. These lattice parameters are slightly larger than those of Nb_2AlC (*a* = 3.096-3.126 Å and *c* = 13.804-13.888 Å).[39] The difference can be ascribed to the larger metallic radius of Sc (160 pm) compared to Nb (145 pm).[40] Similarly, and likely for the same reason, the lattice parameters of $(Nb_{2/3}Sc_{1/3})_4AlC_3$ (*a* = 3.1855(5) Å and *c* = 23.878(6) Å) are slightly larger than those of Nb_4AlC_3 (*a* = 3.1296 Å and *c* = 24.1208 Å).[41] Despite the fact that to date Nb_3AlC_2 has not been experimentally realized, the introduction of Sc appears

to stabilize the $(Nb_{2/3}Sc_{1/3})_3AlC_2$ solid solution. This has been also reported for other 312 phases, where a second M element stabilizes an otherwise unstable 312 phase.[42-43]

According to Energy Dispersive X-ray Spectroscopy (EDS) of individual MAX phase particles assumed to be $(Nb_{2/3}Sc_{1/3})_2AlC$, the Nb:Sc:Al atomic ratio was 1.2:0.8:1.0 (details of EDS analysis can be found in Supporting Information). From the Rietveld refinment of the Nb and Sc occupancies in the same phase, the Nb:Sc atomic ratio was found to be 1.38:0.62. It is thus reasonable to conclude the Nb:Sc ratio is between 1.2:0.8 and 1.4:0.6. At 2:1.33 to 2:0.86, respectively, these ratios bracket the nominal ratio of 2:1.

The MXene synthesis details can be found in the Supporting Information. Immersing $(Nb_{2/3}Sc_{1/3})_2AlC$ powders in 48% conc. hydrofluoric acid (HF) at room temperature, RT, for 30 h resulted in selective etching of the majority of both of the Al and Sc atoms, creating $Nb_{1.33}CT_x$ multilayers, MLs, (Figure 1c). Clearly the Sc atoms are more reactive than the Nb, which is consistent with theoretical calculations that have shown that the Sc-C and C-Al bonds in Sc_2AlC are of comparable strengths and both weaker than the Nb-C or Nb-Al bondsin Nb_2AlC.[44]

To obtain $Nb_{1.33}CT_x$ monolayers, the ML powder was intercalated with tetrabutylammonium hydroxide (TBAOH) in water following the procedure described by Naguib *et al.*,[45] followed by delamination in water by hand shaking, yielding a ≈ 1 mg/ml suspension of, most probably, single MXene flakes in water. To produce a delaminated *d*-Nb_2CT_x suspension starting with Nb_2AlC, using the same method, the etching time had to be increased to 100 h - compared to 30 h for $(Nb_{2/3}Sc_{1/3})_2AlC$ - yielding a colloidal suspension with a concentration of < 0.5 mg/ml. Hence, the introduction of Sc in the MAX phase improves yield and reduces etching time.

When filtering the $Nb_{1.33}CT_x$ and Nb_2CT_x suspensions, only the former formed flexible, free-standing films that were easy to handle. The latter formed a brittle film that could not be peeled off the filter membrane without breaking into small pieces. It is for this reason that no transport properties are reported for this compound.

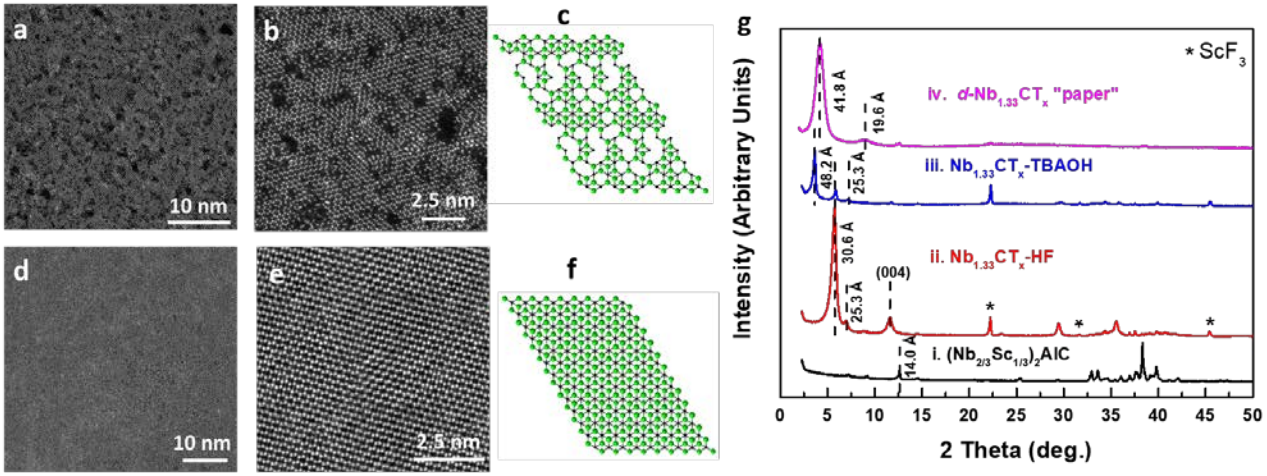

Figure 3. (a) Low magnification STEM micrograph of a $Nb_{1.33}CT_x$ single flake, (b) same as (a) but at higher magnification, (c) top view schematic of single $Nb_{1.33}CT_x$ sheet showing random vacancies and vacancy clusters. d) Low magnification STEM micrograph of Nb_2CT_x single flake, (e) same as (d) but at higher magnification, (f) top view schematic of single Nb_2CT_x sheet and, (g) XRD patterns of, i $(Nb_{2/3}Sc_{1/3})_2AlC$, ii. $Nb_{1.33}CT_x$-HF which is that of multilayers after HF etching of $(Nb_{2/3}Sc_{1/3})_2AlC$ powders, iii. $Nb_{1.33}CT_x$-HF-TBAOH which is $Nb_{1.33}CT_x$ after intercalation with TBAOH, and, iv. d-$Nb_{1.33}CT_x$ film obtained by filtering a suspension of delaminated $Nb_{1.33}CT_x$ (Figure 1e). Peaks annotated by asterisks correspond to ScF_3 which is a residue of etching.

A typical morphology of a $Nb_{1.33}CT_x$ single flake can be seen in the STEM images in Figure 3a,b and can be compared to the schematic shown in Figure 3c. The flakes contain vacancies and vacancy clusters ranging in size between 0.1 and 2 nm, resulting from the removal of the Sc atoms. The vacancies' areal coverage varied from 20% to 35% depending on the area imaged (see Supplementary Information Figure S2). STEM images of Nb_2CT_x single flakes, on the other hand, are shown in Figure 3d,e. In this case, the MXene layers, shown schematically in Figure 3f, are quite visibly less defective. The XRD patterns of the etched material (Figure 3g) show the typical increase in the interlayer spacing, denoted as $d_{c/2}$, (becuase it is ½ the *c-LP* of the (002) parent MAX) to that of the parent phase, (compare Figures 3g-i and ii). This is typical of the MAX to MXene conversion and reflects the substitution of Al with surface terminations of -O, -OH and/or -F and multiple water layers.[45-46] No residual peaks of the parent phase are present after etching indicating a complete MAX to MXene conversion. However, peaks corresponding to ScF_3, denoted by asterisks, were present. After TBAOH intercalation, $d_{c/2}$ increases to 24.1 Å (Figure 3g-iii) reflecting the intercalation of the TBA^+ ions and more water molecules. After filtering the suspension to form a free-standing film (Figure 3g-iv) $d_{c/2}$ is reduced to 20.9 Å presumably due to the removal of some of the water molecules and possibly TBA^+ ions.

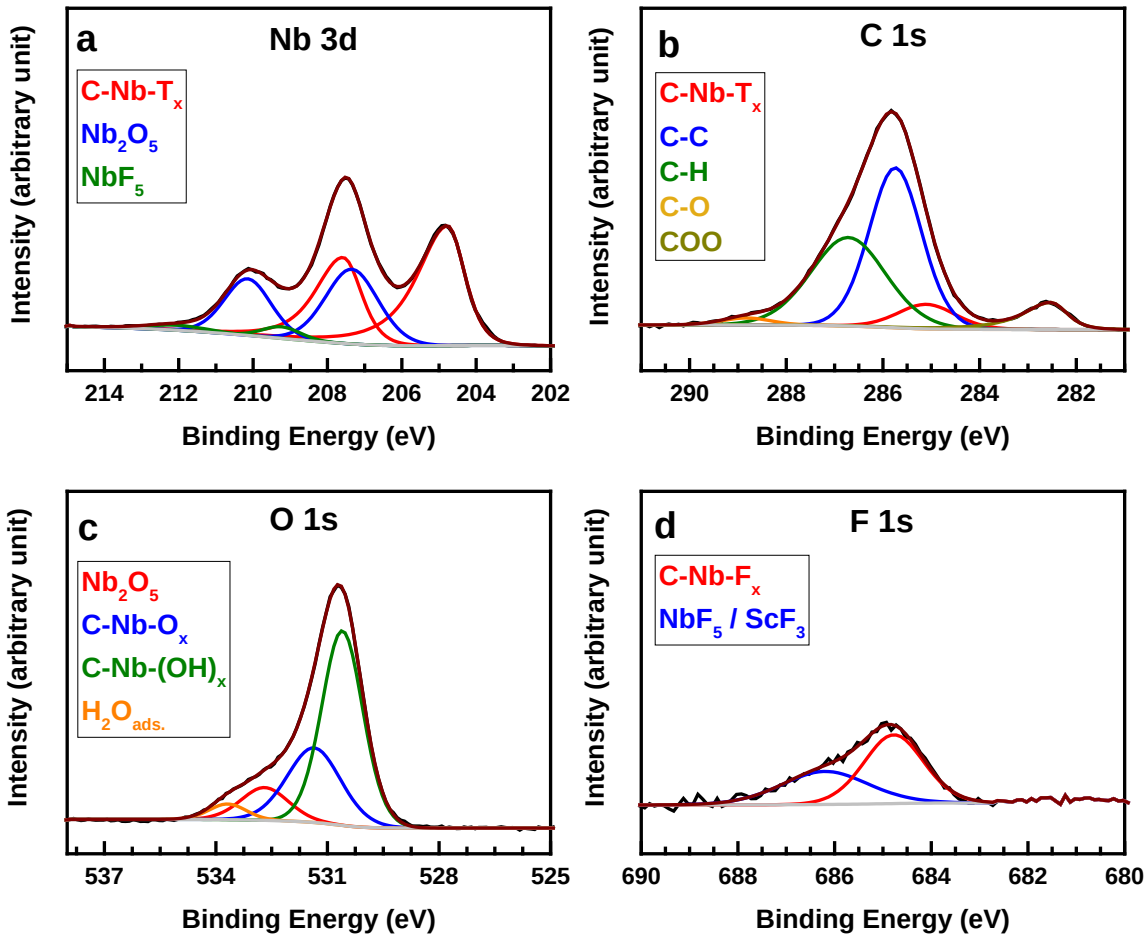

Figure 4. XPS spectra of *d*-$Nb_{1.33}CT_x$ film for, (a) Nb 3d, (b) C 1s, (c) O 1s, and (d) F 1s regions. Color coded fitting peaks represent various assigned species (See Table S4).

High-resolution XPS spectra, with peak fits of a *d*-$Nb_{1.33}CT_x$ filtered film are shown in Figures 4a-d for Nb 3d, C 1s, O 1s, and F 1s regions, respectively. The peak fitting results and the elemental compositions extracted from the high-resolution spectra can be found in Supporting Information. Based on the extracted atomic percentage of Nb, C, O, and F and the fraction of each species solely related to the 2D flakes, the chemical formula that best describes *d*-$Nb_{1.33}CT_x$ is $Nb_{1.33}CO_{1.7}(OH)_{0.6}F_{0.2}.0.2H_2O$, while that for *d*-$Nb_2CT_x$ is $Nb_2CO(OH)_{0.6}F_{0.1}.0.3H_2O$-0.3N. (The C peak associated with MXene was used as the reference with base, error < ± 0.1). The XPS

results for *d*-Nb_2CT_x can be found in Supporting Information. The nitrogen, N, component originates from the intercalated TBAOH, a component that was not possible to extract from the *d*-$Nb_{1.33}CT_x$ flakes due to the overlap between the N 1s and Sc 2p peaks (Figure S3b). it is clear that the -O is the dominant termination for both compounds. Interestingly it is > 1.5 times higher in *d*-$Nb_{1.33}CT_x$ compared to *d*-Nb_2CT_x. The amounts of -OH and –F, are comparable in both samples. Note that the fraction of the -F surface terminations for both compounds is low which is common for MXenes treated with TBAOH.[45-46] At 2.5, the total number of termination moles of for *d*-$Nb_{1.33}CT_x$, is 0.5 higher than the theoretical value of 2 obtained when all surface sites are filled.[47] This suggests that some of the surface terminations may very well reside in the vacancies that result from the removal of the Sc atoms and are thus, strictly speaking, no longer terminations. The total moles of terminations for *d*-Nb_2CT_x, excluding N, is 1.7, which is less than 2.

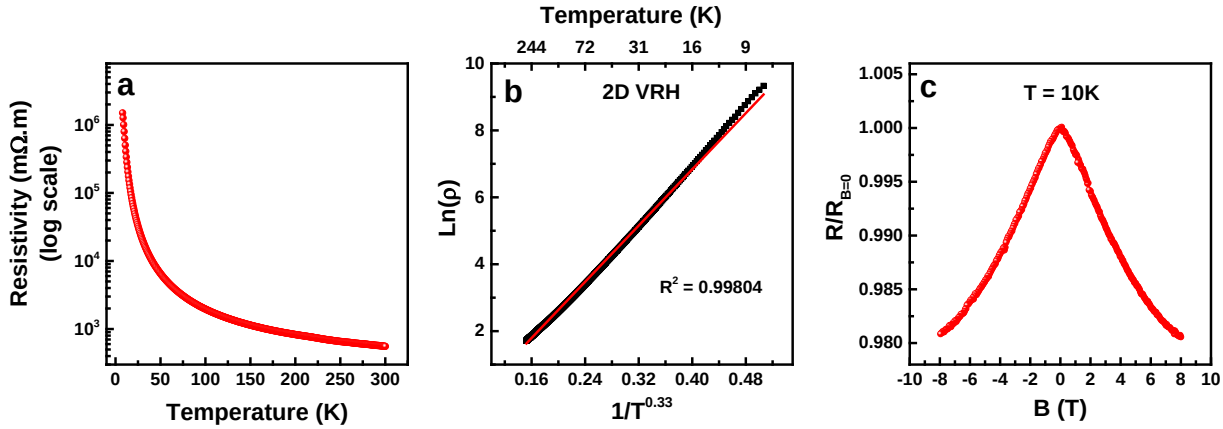

Figure 5. Electronic transport characteristics of *d*-$Nb_{1.33}CT_x$ film on temperature and magnetic field. (a) Log of resistivity, ρ, vs. temperature in 7 to 300 K temperature range, (b) ρ vs. $1/T^{1/3}$ in the 7 to 300 K temperature range assuming 2D variable range hopping (VRH) conduction model and, (c) magnetoresistance at 10 K. $R_{B=0}$ refers to resistance in the absence of magnetic field.

A semi-log plot of the resistivity, ρ, vs. temperature, T, of a 22 μm thick *d*-$Nb_{1.33}CT_x$ film is shown in Figure 5a. The details of the measurements can be found in the Supporting Information. As the temperature decreases from 300 K to 7 K, ρ increases from 0.556 to 1500 Ω.m. To shed more light on the transport mechanism, the ρ data in the 7 to 300 K temperature range were fitted to several models, including 2D, 3D and the Efros-Shklovskii, E-S, variable range hopping, VRH, simple thermal activation and power-law (non-exponential) models. The fitting results (Figure 5b and Figure S5) clearly eliminate the latter two (Figure S5). The same results, however, cannot differentiate between the various VRH models; the R^2 for 2D, E-S and 3D VRH models are comparable, 0.9980, 0.9978 and 0.9964, respectively. Figure 5b plots the results for the most likely model, viz. 2D VRH, the other fits for the other models can be found in Figure S5. Similar behavior has been reported for other MXene films such as Mo_2CT_x,[46] $Mo_2TiC_2T_x$ and $Mo_2Ti_2C_3T_x$.[48]

Magnetoresistance (MR) measurements - performed at 10 K – showed a negative MR, which is in contradistinction with MR measurements on other MXene compounds exhibiting the VRH mechanism.[46, 48] However, other disordered materials showing VRH, such as In_2O_{3-x}, and Si doped in GaAs have been reported to exhibit negative MRs.[49-51] The negative MR for materials having VRH conduction mechanisms has been ascribed to several reasons such as quantum interference, Zeeman effect or localized magnetic moments.[52] These comments notwithstanding, much more work - which is beyond the scope of this paper - is needed to obtain a deeper understanding of conduction in our films.

In conclusion, a facile, reproducible, relatively rapid method for producing random vacancies and vacancy clusters in MXenes is presented, where the minority M element in a quaternary solid solution MAX phase is concomitantly etched with the A-group element. Herein we synthesized $(Nb_{2/3}Sc_{1/3})_2AlC$ and selectively etched both the Sc and Al atoms to produce $Nb_{1.33}CT_x$ with disordered vacancies. The presence of Sc in the quaternary MAX phase decreased the etching time from 100 to 30 h and increased the yield of delaminated flakes.

When $Nb_{1.33}CT_x$ free-standing films were cooled from 300 to 7 K, their resistivity increased from 0.556 to 1500 Ω.m. The suggested transport mechanism is VRH accompanied by a negative MR at 10 K. Lastly, there is no reason this approach cannot be used to "dial-in" a controlled number of vacancies, as long as the parent solid solution MAX phase exists. The fact that the flakes with vacancies are less dense than their counterparts is also noteworthy when specific properties are sought.

ASSOCIATED CONTENT

Supporting Information.

The Supporting Information is available free of charge.

Synthesis of materials, characterization techniques, XPS spectra and transport fitting. (PDF)

AUTHOR INFORMATION

Corresponding Author

* Email: johanna.rosen@liu.se

Author Contributions

J.H. synthetized the material, performed the XRD, XPS characterization and analysis. M.P. performed the transport measurements, M.P., E.J.M, and J.H. analyzed the transport data. J.T. performed the SEM and EDX characterization and analyzed the data. J.P. and J.L performed the STEM characterization and analyzed the data. P.P., M.W.B and J.R. supervised the research. All authors contributed in the preparation of the manuscript and in discussions. All authors have given approval to the final version of the manuscript.

Notes

The authors declare no competing financial interest.

ACKNOWLEDGMENT

We acknowledge support from the Swedish Foundation for Strategic Research (SSF) through the Synergy Grant FUNCASE, the Research Infrastructure Fellow RIF 14-0074, and from the Knut and Alice Wallenberg (KAW) Foundation for a Fellowship Grant, Project funding (KAW

2015.0043), and for support to the Linköping Electron Microscopy Laboratory. The Swedish Research council is gratefully acknowledged through Projects 642-2013-8020 and 621-2014-4890. We also acknowledge the Swedish Government Strategic Research Area in Materials Science on Functional Materials at Linköping University (Faculty Grant SFO-Mat-LiU No. 2009-00971).

REFERENCES

1. Mas-Balleste, R.; Gomez-Navarro, C.; Gomez-Herrero, J.; Zamora, F., 2D Materials: to Graphene and Beyond. *Nanoscale* **2011,** *3*, 20-30.
2. Fiori, G.; Bonaccorso, F.; Iannaccone, G.; Palacios, T.; Neumaier, D.; Seabaugh, A.; Banerjee, S. K.; Colombo, L., Electronics Based on Two-Dimensional Materials. *Nat. Nanotechnol.* **2014,** *9*, 768-779.
3. Choi, M. S.; Lee, G.-H.; Yu, Y.-J.; Lee, D.-Y.; Lee, S. H.; Kim, P.; Hone, J.; Yoo, W. J., Controlled Charge Trapping by Molybdenum Disulphide and Graphene in Ultrathin Heterostructured Memory Devices. *Nature communications* **2013,** *4*, 1624.
4. Bernardi, M.; Palummo, M.; Grossman, J. C., Extraordinary Sunlight Absorption and One Nanometer Thick Photovoltaics Using Two-Dimensional Monolayer Materials. *Nano Lett.* **2013,** *13*, 3664-3670.
5. Surwade, S. P.; Smirnov, S. N.; Vlassiouk, I. V.; Unocic, R. R.; Veith, G. M.; Dai, S.; Mahurin, S. M., Water Desalination Using Nanoporous Single-Layer Graphene. *Nat. Nanotechnol.* **2015,** *10*, 459-464.
6. Bonaccorso, F.; Colombo, L.; Yu, G.; Stoller, M.; Tozzini, V.; Ferrari, A. C.; Ruoff, R. S.; Pellegrini, V., Graphene, Related Two-Dimensional Crystals, and Hybrid Systems for Energy Conversion and Storage. *Science* **2015,** *347*, 1246501.
7. Liu, Z.; Lau, S. P.; Yan, F., Functionalized Graphene and Other Two-Dimensional Materials for Photovoltaic Devices: Device Design and Processing. *Chem. Soc. Rev.* **2015,** *44*, 5638-5679.
8. Wan, J.; Lacey, S. D.; Dai, J.; Bao, W.; Fuhrer, M. S.; Hu, L., Tuning Two-Dimensional Nanomaterials by Intercalation: Materials, Properties and Applications. *Chem. Soc. Rev.* **2016,** *45*, 6742-6765.
9. Amani, M.; Lien, D.-H.; Kiriya, D.; Xiao, J.; Azcatl, A.; Noh, J.; Madhvapathy, S. R.; Addou, R.; Santosh, K.; Dubey, M., Near-unity Photoluminescence Quantum Yield in MoS_2. *Science* **2015,** *350*, 1065-1068.
10. Naguib, M.; Kurtoglu, M.; Presser, V.; Lu, J.; Niu, J. J.; Heon, M.; Hultman, L.; Gogotsi, Y.; Barsoum, M. W., Two-Dimensional Nanocrystals Produced by Exfoliation of Ti_3AlC_2. *Adv. Mater.* **2011,** *23*, 4248-4253.
11. Naguib, M.; Mashtalir, O.; Carle, J.; Presser, V.; Lu, J.; Hultman, L.; Gogotsi, Y.; Barsoum, M. W., Two-Dimensional Transition Metal Carbides. *ACS Nano* **2012,** *6*, 1322-31.
12. Zhou, J.; Zha, X.; Chen, F. Y.; Ye, Q.; Eklund, P.; Du, S.; Huang, Q., A Two-Dimensional Zirconium Carbide by Selective Etching of Al_3C_3 from Nanolaminated $Zr_3Al_3C_5$. *Angew. Chem.* **2016,** *128*, 5092-5097.

13. Barsoum, M. W., *MAX Phases: Properties of Machinable Ternary Carbides and Nitrides*. John Wiley & Sons **2013**.
14. Halim, J.; Lukatskaya, M. R.; Cook, K. M.; Lu, J.; Smith, C. R.; Näslund, L.-Å.; May, S. J.; Hultman, L.; Gogotsi, Y.; Eklund, P.; Barsoum, M. W., Transparent Conductive Two-Dimensional Titanium Carbide Epitaxial Thin Films. *Chem. Mater.* **2014**, *26*, 2374-2381.
15. Ghidiu, M.; Lukatskaya, M. R.; Zhao, M.-Q.; Gogotsi, Y.; Barsoum, M. W., Conductive Two-Dimensional Titanium Carbide `Clay' with High Volumetric Capacitance. *Nature* **2014,** *516*, 78-81.
16. Ghidiu, M.; Halim, J.; Kota, S.; Bish, D.; Gogotsi, Y.; Barsoum, M. W., Ion-Exchange and Cation Solvation Reactions in Ti_3C_2 MXene. *Chem. Mater.* **2016**, *28*, 3507-3514.
17. Liu, F.; Zhou, J.; Wang, S.; Wang, B.; Shen, C.; Wang, L.; Hu, Q.; Huang, Q.; Zhou, A., Preparation of High-Purity V_2C MXene and Electrochemical Properties as Li-Ion Batteries. *J. Electrochem. Soc.* **2017,** *164*, A709-A713.
18. Halim, J.; Cook, K. M.; Naguib, M.; Eklund, P.; Gogotsi, Y.; Rosen, J.; Barsoum, M. W., X-Ray Photoelectron Spectroscopy of Select Multi-layered Transition Metal Carbides (MXenes). *Appl. Surf. Sci.* **2016,** *362*, 406-417.
19. Ng, V. M. H.; Huang, H.; Zhou, K.; Lee, P. S.; Que, W.; Xu, J. Z.; Kong, L. B., Recent Progress in Layered Transition Metal Carbides and/or Nitrides (MXenes) and their Composites: Synthesis and Applications. *Journal of Materials Chemistry A* **2017,** *5*, 3039-3068.
20. Lukatskaya, M. R.; Kota, S.; Lin, Z.; Zhao, M.-Q.; Shpigel, N.; Levi, M. D.; Halim, J.; Taberna, P.-L.; Barsoum, M. W.; Simon, P., Ultra-high-rate Pseudocapacitive Energy Storage in Two-Dimensional Transition Metal Carbides. *Nature Energy* **2017,** *2*, 17105.
21. Halim, J.; Lukatskaya, M. R.; Cook, K. M.; Lu, J.; Smith, C. R.; Näslund, L.-Å.; May, S. J.; Hultman, L.; Gogotsi, Y.; Eklund, P., Transparent Conductive Two-Dimensional Titanium Carbide Epitaxial Thin Films. *Chem. Mater.* **2014,** *26*, 2374-2381.
22. Naguib, M.; Mochalin, V. N.; Barsoum, M. W.; Gogotsi, Y., 25^{th} Anniversary Article: MXenes: A New Family of Two-Dimensional Materials. *Adv. Mater.* **2014,** *26*, 992-1005.
23. Anasori, B.; Lukatskaya, M. R.; Gogotsi, Y., 2D Metal Carbides and Nitrides (MXenes) for Energy Storage. *Nature Reviews Materials* **2017,** *2*, 16098.
24. Eklund, P.; Rosen, J.; Persson, P. O. Å., Layered Ternary $M_{n+1}AX_n$ Phases and their 2D Derivative MXene: An Overview from a Thin-film Perspective. *J. Phys. D: Appl. Phys.* **2017,** *50*, 113001.
25. Sun, S.; Liao, C.; Hafez, A. M.; Zhu, H.; Wu, S., Two-Dimensional MXenes for Energy Storage. *Chem. Eng. J. (Lausanne)* **2017**, *15*, 27-45.
26. Naguib, M.; Bentzel, G. W.; Shah, J.; Halim, J.; Caspi, E. N.; Lu, J.; Hultman, L.; Barsoum, M. W., New Solid Solution MAX Phases: $(Ti_{0.5}, V_{0.5})_3AlC_2$, $(Nb_{0.5}, V_{0.5})_2AlC$, $(Nb_{0.5}, V_{0.5})_4AlC_3$ and $(Nb_{0.8}, Zr_{0.2})_2AlC$. *Materials Research Letters* **2014,** *2*, 233-240.
27. Manoun, B.; Saxena, S.; Hug, G.; Ganguly, A.; Hoffman, E.; Barsoum, M., Synthesis and Compressibility of $Ti_3(Al, Sn_{0.2})C_2$ and $Ti_3Al(C_{0.5}, N_{0.5})_2$. *J. Appl. Phys.* **2007,** *101*, 113523.
28. Yang, J.; Naguib, M.; Ghidiu, M.; Pan, L.-M.; Gu, J.; Nanda, J.; Halim, J.; Gogotsi, Y.; Barsoum, M. W., Two-Dimensional Nb-Based M_4C_3 Solid Solutions (MXenes). *J. Am. Ceram. Soc.* **2015**, *99*, 660-666.
29. Dall'Agnese, Y.; Lukatskaya, M. R.; Cook, K. M.; Taberna, P.-L.; Gogotsi, Y.; Simon, P., High Capacitance of Surface-modified 2D Titanium Carbide in Acidic Electrolyte. *Electrochem. Commun.* **2014,** *48*, 118-122.

30. Persson, I.; Näslund, L.-Å.; Halim, J.; Barsoum, M. W.; Darakchieva, V.; Palisaitis, J.; Rosen, J.; Persson, P. O. Å., On the Organization and Thermal Behavior of Functional Groups on Ti_3C_2 MXene Surfaces in Vacuum. *2D Materials* **2017,** *5*, 015002.
31. Tao, Q.; Dahlqvist, M.; Lu, J.; Kota, S.; Meshkian, R.; Halim, J.; Palisaitis, J.; Hultman, L.; Barsoum, M. W.; Persson, P. O., Two-dimensional $Mo_{1.33}C$ MXene with Divacancy Ordering Prepared from Parent 3D Laminate with In-plane Chemical Ordering. *Nature communications* **2017,** *8*, 14949.
32. Qin, L.; Tao, Q.; El Ghazaly, A.; Fernandez-Rodriguez, J.; Persson, P. O. Å.; Rosen, J.; Zhang, F., High-Performance Ultrathin Flexible Solid-State Supercapacitors Based on Solution Processable $Mo_{1.33}C$ MXene abd PEDOT:PSS. *Adv. Funct. Mater.* **2017,** *28*, 1703808.
33. Dahlqvist, M.; Lu, J.; Meshkian, R.; Tao, Q.; Hultman, L.; Rosen, J., Prediction and Synthesis of a Family of Atomic Laminate Phases with Kagomé-like and In-plane Chemical Ordering. *Science Advances* **2017,** *3*, 1700642.
34. Lu, J.; Thore, A.; Meshkian, R.; Tao, Q.; Hultman, L.; Rosen, J., Theoretical and Experimental Exploration of a Novel In-plane Chemically-ordered $(Cr_{2/3}M_{1/3})_2AlC$ i-MAX Phase with M= Sc and Y. *Cryst. Growth Des.* **2017**, *17*, 5704-5711.
35. Lin, H.; Gao, S.; Dai, C.; Chen, Y.; Shi, J., Two-Dimensional Biodegradable Niobium Carbide (MXene) for Photothermal Tumor Eradication in NIR-I and NIR-II Bio-Windows. *J. Am. Chem. Soc.* **2017**, *139*, 16235-16247.
36. Mashtalir, O.; Lukatskaya, M. R.; Zhao, M. Q.; Barsoum, M. W.; Gogotsi, Y., Amine-assisted Delamination of Nb_2C MXene for Li-Ion Energy Storage Devices. *Adv. Mater.* **2015,** *27*, 3501-3506.
37. Naguib, M.; Halim, J.; Lu, J.; Cook, K. M.; Hultman, L.; Gogotsi, Y.; Barsoum, M. W., New Two-dimensional Niobium and Vanadium Carbides as Promising Materials for Li-ion Batteries. *J. Am. Chem. Soc.* **2013,** *135*, 15966-9.
38. Su, T.; Peng, R.; Hood, Z. D.; Naguib, M.; Ivanov, I. N.; Keum, J. K.; Qin, Z.; Guo, Z.; Wu, Z., One-step Synthesis of $Nb_2O_5/C/Nb_2C$ (MXene) Composites and their Use as Photocatalysts for Hydrogen Evolution. *ChemSusChem* **2017**, *11*, 688-699.
39. Salama, I.; El-Raghy, T.; Barsoum, M. W., Synthesis and Mechanical Properties of Nb_2AlC and $(Ti,Nb)_2AlC$. *J. Alloys Compd.* **2002,** *347*, 271-278.
40. Cordero, B.; Gómez, V.; Platero-Prats, A. E.; Revés, M.; Echeverría, J.; Cremades, E.; Barragán, F.; Alvarez, S., Covalent Radii Revisited. *Dalton Trans.* **2008,** (21), 2832-2838.
41. Hu, C.; Li, F.; Zhang, J.; Wang, J.; Wang, J.; Zhou, Y., Nb_4AlC_3: A New Compound Belonging to the MAX Phases. *Scr. Mater.* **2007,** *57*, 893-896.
42. Halim, J.; Chartier, P.; Basyuk, T.; Prikhna, T.; El'ad, N. C.; Barsoum, M. W.; Cabioc'h, T., Structure and Thermal Expansion of $(Cr_x, V_{1-x})_{n+1}AlC$ n Phases Measured by X-Ray Diffraction. *J. Eur. Ceram. Soc.* **2017,** *37*, 15-21.
43. Zhou, Y.; Meng, F.; Zhang, J., New MAX-Phase Compounds in the V–Cr–Al–C System. *J. Am. Ceram. Soc.* **2008,** *91*, 1357-1360.
44. Khazaei, M.; Ranjbar, A.; Esfarjani, K.; Bogdanovski, D.; Dronskowski, R.; Yunoki, S., Insights into Exfoliation Possibility of MAX Phases to MXenes. *Phys. Chem. Chem. Phys.* **2018**, *20*, 8579-8592.
45. Naguib, M.; Unocic, R. R.; Armstrong, B. L.; Nanda, J., Large-scale Delamination of Multi-layers Transition Metal Carbides and Carbonitrides "MXenes". *Dalton Trans.* **2015,** *44*, 9353-8.

46. Halim, J.; Kota, S.; Lukatskaya, M. R.; Naguib, M.; Zhao, M. Q.; Moon, E. J.; Pitock, J.; Nanda, J.; May, S. J.; Gogotsi, Y., Synthesis and Characterization of 2D Molybdenum Carbide (MXene). *Adv. Funct. Mater.* **2016**, *26*, 3118-3127.
47. Ashton, M.; Mathew, K.; Hennig, R. G.; Sinnott, S. B., Predicted Surface Composition and Thermodynamic Stability of MXenes in Solution. *The Journal of Physical Chemistry C* **2016,** *120*, 3550-3556.
48. Anasori, B.; Shi, C.; Moon, E. J.; Xie, Y.; Voigt, C. A.; Kent, P. R.; May, S. J.; Billinge, S. J.; Barsoum, M. W.; Gogotsi, Y., Control of Electronic Properties of 2D Carbides (MXenes) by Manipulating their Transition Metal Layers. *Nanoscale Horizons* **2016,** *1*, 227-234.
49. Jiang, H.; Johnson, C.; Wang, K., Giant Negative Magnetoresistance of a Degenerate Two-Dimensional Electron Gas in the Variable-range-hopping Regime. *Phys Rev B* **1992,** *46*, 12830.
50. Zhao, H. L.; Spivak, B. Z.; Gelfand, M. P.; Feng, S., Negative Magnetoresistance in Variable-range-hopping conduction. *Phys Rev B* **1991,** *44* (19), 10760.
51. Gu, H.; Guo, J.; He, Q.; Jiang, Y.; Huang, Y.; Haldolaarachige, N.; Luo, Z.; Young, D. P.; Wei, S.; Guo, Z., Magnetoresistive Polyaniline/multi-walled Carbon Nanotube Nanocomposites with Negative Permittivity. *Nanoscale* **2014,** *6*, 181-189.
52. Sybous, A.; El Kaaouachi, A.; Hemine, J.; Narjis, A.; Limouny, L.; Dlimi, S.; Abdia, R.; Biskupski, G., Negative Magnetoresistance Behaviour and Variable Range Hopping Conduction in Insulating NbSi Amorphous Alloys at Very Low Temperature with Magnetic Field. *Journal of Modern Physics* **2012,** *3*, 521.

TOC

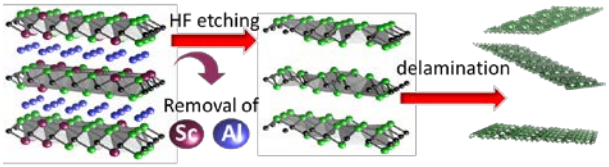

Supporting Information

Synthesis of two-dimensional $Nb_{1.33}C$ (MXene) with randomly distributed vacancies by etching a $(Nb_{2/3}Sc_{1/3})_2AlC$ solid solution

*J. Halim,[a] J. Palisaitis,[a] J. Lu,[a] J. Thörnberg,[a] E.J. Moon,[b] M. Precner,[c] P. Eklund, P. O. Å. Persson,[a] M. W. Barsoum,[b] and J. Rosen[a,]**

[a] Thin Film Physics, Department of Physics, Chemistry, and Biology (IFM), Linkoping, Sweden

[b] Department of Materials Science and Engineering, Drexel University, PA 19104, USA

[c] Institute of Electrical Engineering, Slovak Academy of Sciences, 84104 Bratislava, Slovak Republic

Corresponding author: *johanna.rosen@liu.se

1. Materials and methods

1.1 MAX and MXene synthesis

Synthesis of $(Nb_{2/3}Sc_{1/3})_2AlC$: Powders of $(Nb_{2/3}Sc_{1/3})_2AlC$ were synthesized by a solid state reaction of elemental powders. Powders of Nb (99.8%, 325 mesh, Alfa Aesar, Kandel, Germany), Sc (99.99%, Standford Advanced Material, USA), Al (99.5%, 325 mesh, Alfa Aesar, Kandel, Germany) and C (99.9995%, 200 mesh, Alfa Aesar, Karlsruhe, Germany) were placed in an agate mortar in a 4/3:2/3:1:1 molar ratio and manually mixed. After mixing they was poured in a Teflon jar and hand shaken for 5 min. The mixture was heated at a rate of 5 °C/min to 1400 °C in an alumina crucible under 5 sccm Ar flow and held at 1400 °C for 2 h. After furnace cooling, the lightly sintered sample was crushed, using the agate mortar and pestle and sieved through a 450 mesh sieve.

Synthesis of Nb_2AlC: Powders of *Nb_2AlC* were synthesized by a solid state reaction of elemental powders as detailed in Ref.[1] In short, powders of Nb (99.8%, 325 mesh, Alfa Aesar, Kandel, Germany), Al (99.5%, 325 mesh, Alfa Aesar, Kandel, Germany) and C (99.9995%, 200 mesh, Alfa Aesar, Karlsruhe, Germany) were mixed as above and heated at a rate of 5 °C/min to 1600 °C in an alumina crucible under 5 sccm Ar flow and held at 1600 °C for 2 h. After furnace cooling, the lightly sintered sample was crushed, using the agate mortar and pestle and sieved through a 450 mesh sieve.

Synthesis of 2D $Nb_{1.33}CT_x$: Two grams of $(Nb_{2/3}Sc_{1/3})_2AlC$ powder were slowly added to a Teflon bottle containing 40 ml of 48% aqueous HF (Honeywell Fluka, Sweden). The bottle containing the mixture was placed on a stir plate at room temperature and the mixture was stirred using a Teflon coated magnet for 30 h. The resulting suspension was washed with DI water for several cycles till the a pH of ≈ 6 was reached. In each washing cycle 40 ml of DI water were added to the mixture in a centrifuge tube and the tube was hand-shaken for 1 min before centrifuging at 5000 rpm for 1 min. The settled powder was removed from the centrifuge tube and filtered through a nanoporous polypropylene membrane (3501 Coated PP, 0.064 µm pore size, Celgard, LLC, USA) for further investigation.

One gram of the filtered powder was added to a 5 ml of an aqueous solution of 54-56 wt.% TBAOH, $(C_4H_9)_4NOH$, (Sigma Aldrich, Sweden). The mixture was hand-shaken for 5 min then washed 3 times by 40 ml DI each time; the resulting sediment was used for further characterization and delamination.

To obtain a delaminated $Nb_{1.33}CT_x$ colloidal suspension and free-standing films, the TBAOH intercalated powder was mixed with water (1 g $Nb_{1.33}CT_x$ per 50 ml of DI water) and hand-shaken for 5 min. Then the mixture was centrifuged for 1 h at 5000 rpm and the supernatant - which was comprised of, presumably, single or few delaminated $Nb_{1.33}CT_x$ flakes at a concentration of 1 mg/ml - was collected. The suspension was then vacuum-filtered onto a nanoporous polypropylene membrane (3501 Coated PP, 0.064 µm pore size, Celgard, LLC, USA) in air. The delaminated *d*-$Nb_{1.33}CT_x$ "paper" was easily separated from the membrane to obtain free-standing, flexible $Nb_{1.33}CT_x$ films.

Synthesis of 2D Nb_2CT_x: Two grams of Nb_2AlC powder were slowly immersed in a Teflon bottle containing 20 ml of 48% aqueous HF. The bottle containing the mixture was placed on a stir plate at room temperature and the mixture was stirred using a Teflon coated magnet for 100 hr. The resulting suspension was washed with DI water for several cycles till the mixture reached a pH of ≈ 6. In each washing cycle 40 ml of DI water were added to the mixture in a centrifuge tube and the tube was hand-shaken for 1 min before centrifuging at 5000 rpm for 1

min. The settled powder was removed from the centrifuge tube and filtered through a nanoporous polypropylene membrane for further investigation.

One gram of the filtered powdered was added to a 5 ml of an aqueous solution of 54-56 wt.% TBAOH, $(C_4H_9)_4NOH$. The mixture was hand-shaken for 5 min then washed 3 times by 40 ml DI each time and the sediment was used for further characterization and delamination.

To obtain a Nb_2CT_x colloidal suspension and free-standing film, the TBAOH intercalated powder was mixed with water (1 g Nb_2CT_x per 50 ml of DI water) and sonicated using an ultra-sonication bath for 1 h. Sonication was performed while the mixture was bubbled with N_2 gas. The mixture was then centrifuged for 1 h at 5000 rpm and the supernatant - which was comprised of, presumably, single or few delaminated $Nb_{1.33}CT_x$ flakes at a concentration of 0.5 mg/ml - was collected. The suspension was then vacuum-filtered onto nanoporous polypropylene membrane in air. Unfortunately, the delaminated *d*-Nb_2CT_x "paper" was stuck to the membrane and attempts to separate the two from each other resulted in the breakdown of the film into small brittle pieces.

1.2 Materials characterization

The microstructures and morphologies of the MAX and MXene samples were characterized by Scanning Transmission Electron Microscope (STEM) combined with high angle annular dark field imagining (STEM-HAADF) in a double-corrected Linköping FEI Titan^3 60-300, operated at both 300 kV and 60 kV and Transmission Electron Microscopy (TEM) FEI Tecnai T20 operated at 200 kV accompanied with Selected Area Electron Diffraction (SAED). The MAX phase sample was prepared by embedding the ground-mixed powder in a Cu grid with a carbon film. For the delaminated MXene flakes, a few from a water suspension were drop cast on to the Cu grid with carbon film.

Scanning Electron Microscopy (SEM) imaging was performed using a SEM LEO 1550 Gemini operated with an acceleration voltage between 5 and 15 keV equipped with an Oxford INCA Energy E2H X-ray Energy Dispersive Spectrometer (EDS) system with Silicon Drifted detector.

X-ray diffraction (XRD) was carried out on a PANalytical X'Pert powder diffraction, with Cu source ($\lambda_{K\alpha} \approx 1.54$ Å). A graded Bragg-Brentano with a 1/4° divergent and 1/2° anti-scatter slits, and a 5 mm anti-scatter slit together with a Soller slit (with an opening of 0.04 radian), in the incident and the diffracted beam sides were used, respectively.

The XRD pattern of the $(Nb_{2/3}Sc_{1/3})_2AlC$ powder was analysed by the Rietveld refinement method, using the *FULLPROF* code.[2-3] Refined parameters were scale factors from which relative phase fractions were evaluated, *X* and *Y* profile parameters for peak width, lattice parameters (LPs) and atomic positions for all phases in addition to the occupancies of Nb and Sc atoms in the $(Nb_{2/3}Sc_{1/3})_2AlC$ and Nb and Sc atoms in $(Nb_{2/3}Sc_{1/3})_3AlC_2$ occupying the atomic position (0.333, 0.667, 0.122). The background was refined via linear extrapolation of a manually selected background.

X-ray photoelectron spectroscopy (XPS) measurements were performed on a free-standing *d*-$Nb_{1.33}CT_x$ film and a *d*-Nb_2CT_x film stuck on the filter membrane using a surface analysis system (Kratos AXIS Ultra^{DLD}, Manchester, U.K.) with monochromatic Al-Kα (1486.6 eV) radiation. Each sample was mounted on a double-sided tape and grounded to the sample stage with copper contacts. The X-ray beam irradiated the sample surface at an angle of 45º, with respect to the surface and provided an X-ray spot of ≈ 300 x 800 µm. Charge neutralization was performed using a co-axial, low energy (~0.1 eV) electron flood source to avoid shifts in the recorded binding energy (BE). XPS spectra were recorded for F 1s, O 1s, C 1s, Al 2p, and Nb 3d and Sc 2p. The analyser pass energy used for all the regions was 20 eV with a step size of 0.1 eV. The BE scale of all XPS spectra was referenced to the Fermi-edge (E_F), which was set

to a BE of zero eV. The peak fitting was carried out using CasaXPS Version 2.3.16 RP 1.6 in the same manner as in references [4-7]. The global elemental percentage was quantified as in references[4-7].

The temperature-dependent in-plane resistivity measurements were performed in a Physical Property Measurement System (PPMS) controlled by the Model 6000 for temperatures from 1.9 to 400 K and external magnetic field up to 14 T.

2. Results for the Rietveld refinement of the XRD pattern of $(Nb_{2/3}Sc_{1/3})_2AlC$ powder

Table S1. Rietveld refinement of $(Nb_{2/3}Sc_{1/3})_2AlC$, $(Nb_{2/3}Sc_{1/3})_3AlC_2$ and $(Nb_{2/3}Sc_{1/3})_4AlC_3$ phases of XRD pattern shown in **Fig. 1e.** The mass fractions of the different phases were: $(Nb_{2/3}Sc_{1/3})_2AlC$ (68(2) wt.%), $NbAl_3$ (10.1(4) wt.%), NbC (17.4(4) wt.%), $(Nb_{2/3}Sc_{1/3})_3AlC_2$ (2.5(3) wt.%) and $(Nb_{2/3}Sc_{1/3})_4AlC_3$ (2.0(2) wt.%). The total χ^2 value was 8.78.

	$(Nb_{2/3}Sc_{1/3})_2AlC$	$(Nb_{2/3}Sc_{1/3})_3AlC_2$	$(Nb_{2/3}Sc_{1/3})_4AlC_3$
Space group	*P 63/mmc*	*P 63/mmc*	*P 63/mmc*
Lattice constants (Å)	*a: 3.12915(5)* *c: 13.9736(3)*	*a: 3.0213(3)* *c: 19.116(4)*	*a: 3.1855(5)* *c: 23.878(6)*
Nb and Sc	*4f (0.33333 0.66667 0.0903(1))* *Occupancy of Nb = 2.769(7) and Sc = 1.231(7)*	*4f (0.33333 0.66667 0.122(1))* *Occupancy of Nb = 2.63(3) and Sc = 1.37(3)* *2a (0.000 0.000 0.000)* *Occupancy of Nb = 1.333 and Sc = 0.666*	*4f (0.33333 0.66667 0.0570(9))* *Occupancy of Nb = 2.667 and Sc = 1.33* *4e (0.0000 0.0000 0.1669(8))* *Occupancy of Nb = 2.667 and Sc = 1.33*
Al	*2d (0.667 0.333 0.250)*	*2b (0.667 0.333 0.250)*	*2c (0.667 0.333 0.25)*
C	*2a (0.000 0.000 0.000)*	*4f (0.000 0.000 0.503)*	*4f (0.667 0.333 0.11640)* *2a (0.000 0.000 0.000)*

3. EDS for $(Nb_{2/3}Sc_{1/3})AlC_2$

Table S2. Elemental composition of $(Nb_{2/3}Sc_{1/3})AlC_2$ MAX obtained by EDS, excluding C. The elemental composition was taken by averaging the elemental composition of 10 particles.

Element	Nb	Sc	Al
Atomic %	40.5±1.0	27.0±0.7	32.5±0.8

4. Electron Energy Loss Spectra for $Nb_{1.33}CT_x$ single flake

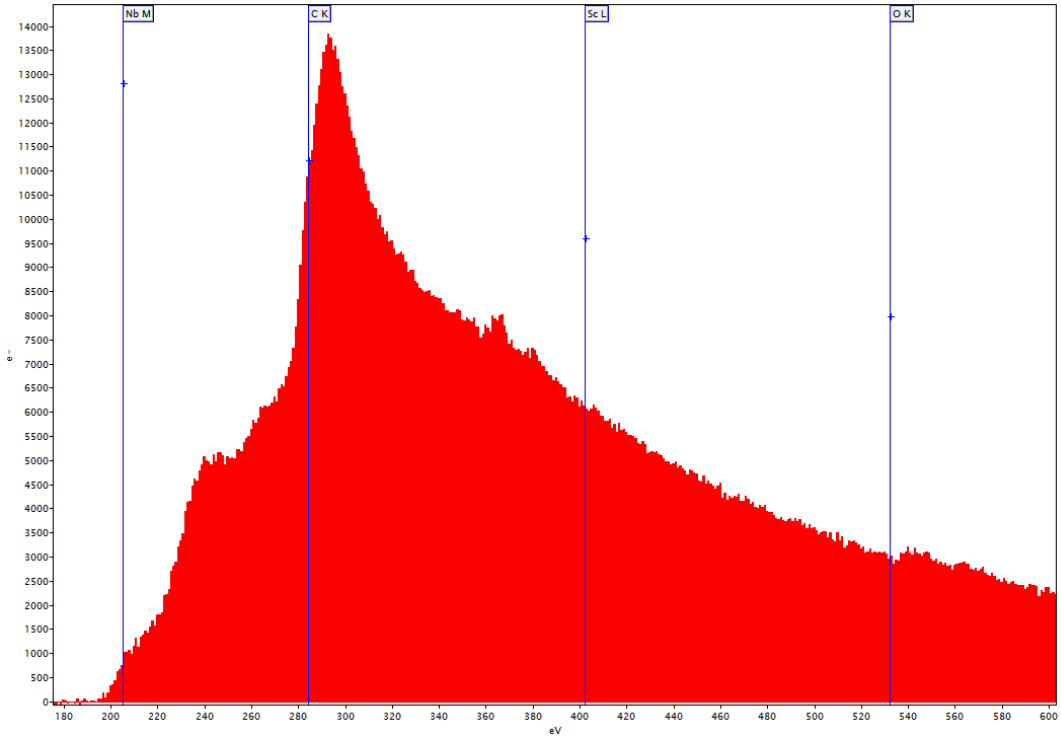

Figure S1. Typical EELS spectra showing Nb-M, C-K and O-K edges from a $Nb_{1.33}CT_x$ single flake.

5. Statistical image analysis of vacancy clusters in a single $Nb_{1.33}CT_x$ flake

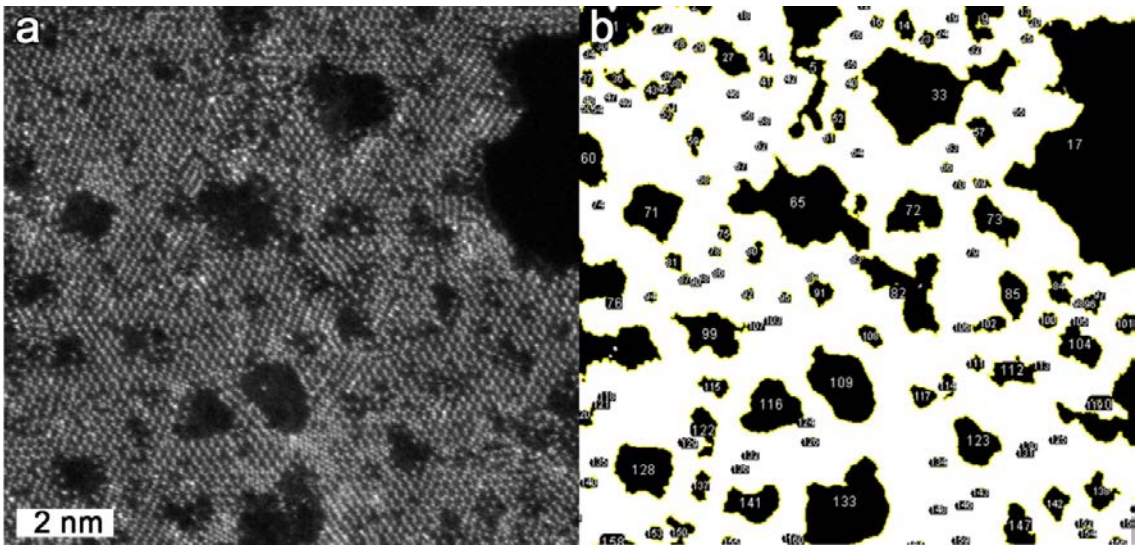

Figure S2. Statistical analysis performed by ImageJ on (a) HRSTEM image obtained from a single $Nb_{1.33}CT_x$ flake. (b) mapped out defects (as black areas) which are covering 30% of the overall image area.

6. XPS analysis of *d*-$Nb_{1.33}CT_x$ and *d*-Nb_2CT_x free-standing films

Table S3. Summary of elemental global atomic percentages for MXenes

	Nb	C	O	F	Al	N
$Nb_{1.33}CT_x$	12.9±0.04	58.7±0.7	26.8±0.3	1.7±0.1	< 0.1	
Nb_2CT_x	19.3±0.08	51.1±1.0	26.8±0.3	0.8±0.1	< 0.1	2.0±0.3

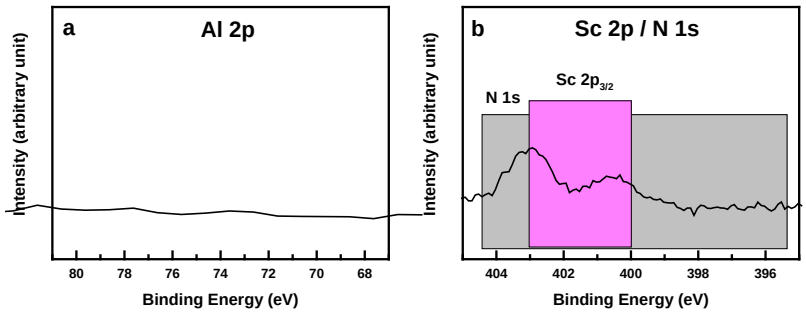

Figure S3. XPS spectra of *d*-$Nb_{1.33}CT_x$ "paper" for (a) Al 2p, and (b) N 1s.

Table S4. XPS peak fitting results for a *d*-$Nb_{1.33}CT_x$ free-standing film. The numbers in parenthesis in column 2 for the Nb 3d region are peak locations of Nb $3d_{3/2}$; their respective FWHMs are listed in column 3 in parenthesis.

Region	BE [eV][a]	FWHM [eV][a]	Fraction	Assigned to	Reference
Nb $3d_{5/2}$ ($3d_{3/2}$)	205.0 (207.8)	1.6 (1.7)	0.48	C-Nb-T_x	[8-9]
	207.6 (210.4)	1.3 (1.3)	0.49	Nb_2O_5	[8, 10-11]
	209.7 (212.5)	1.2 (1.8)	0.03	NbF_5	[12]
C 1s	282.5	0.8	0.08	C-Nb-T_x	[13]
	285.1	1.4	0.08	C-C	[14]
	285.7	1.3	0.46	CH_x	[14]
	286.7	1.8	0.36	C-O	[14]
	288.8	1.2	0.02	COO	[14]
O 1s	530.6	1.3	0.56	Nb_2O_5	[15-18]
	531.4	1.7	0.28	C-Nb-O_x	[18]
	532.7	1.5	0.11	C-Nb-$(OH)_x$	[18]
	533.7	1.3	0.05	H_2O_{ads}	[18]
F 1s	684.8	1.5	0.59	C-Nb-F_x	
	686.2	2.1	0.41	NbF_3 and/or ScF_3	[12, 19]

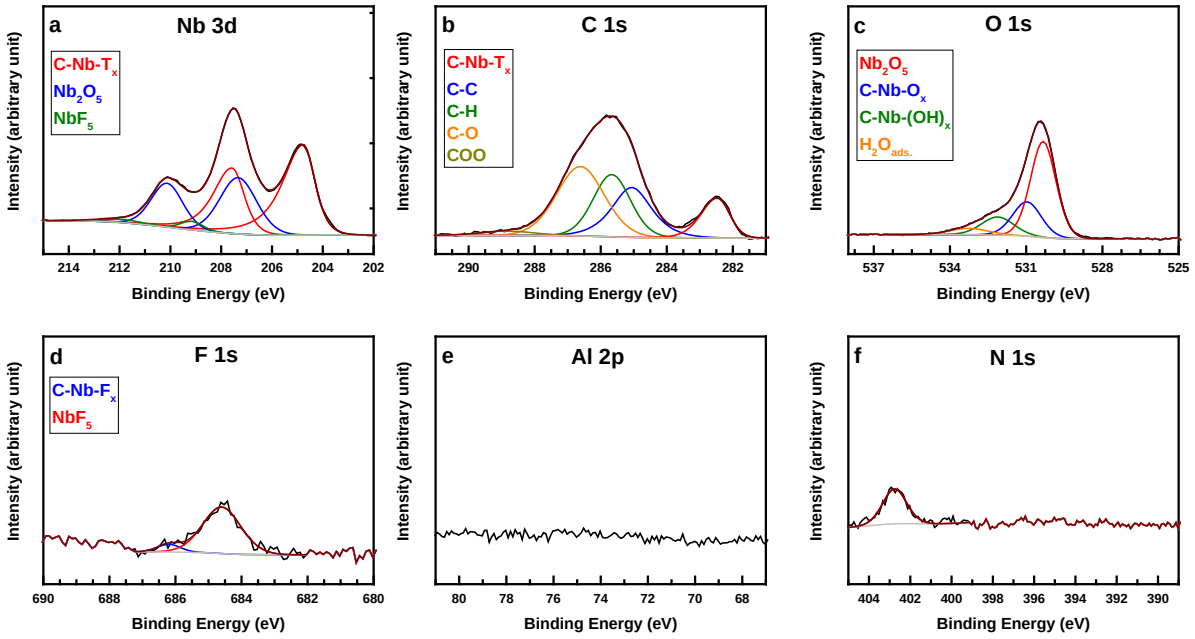

Figure S4. XPS spectra of *d*-Nb_2CT_x free-standing film for, (a) Nb 3d, (b) C 1s, (c) O 1s, (d) F 1s, (e) Al 2p, and, (f) N 1s. Color coded fitting peaks represent various assigned species (See Table S5).

Table S5. XPS peak fitting results for delaminated Nb_2CT_x free-standing film. The numbers in parenthesis in column 2 for the Nb 3d region are peak locations of Nb $3d_{3/2}$; their respective FWHMs are listed in column 3 in parenthesis.

Region	BE [eV][a]	FWHM [eV][a]	Fraction	Assigned to	Reference
Nb $3d_{5/2}$ ($3d_{3/2}$)	204.8 (207.6)	1.1 (1.2)	0.60	C-Nb-T_x	[8-9]
	207.3 (210.1)	1.7 (1.5)	0.37	Nb_2O_5	[8, 10-11]
	209.2 (212.0)	1.0 (1.9)	0.03	NbF_5	[12]
C 1s	282.5	0.9	0.13	C-Nb-T_x	[13]
	285.1	1.4	0.23	C-C	[14]
	285.7	1.3	0.25	CH_x	[14]
	286.6	1.7	0.36	C-O	[14]
	288.8	1.9	0.03	COO	[14]
O 1s	530.3	1.2	0.57	Nb_2O_5	[15-18]
	531.0	1.3	0.23	C-Nb-O_x	[18]
	532.1	1.5	0.14	C-Nb-$(OH)_x$	[18]
	533.3	1.8	0.06	H_2O_{ads}	[18]
F 1s	684.6	1.4	0.91	C-Nb-F_x	
	686.2	1.0	0.09	NbF_5	[12, 19]
N 1s	402.8	1.4	1.0	TBA^+	20

7. Transport analysis of *d*-$Nb_{1.33}CT_x$ free-standing films

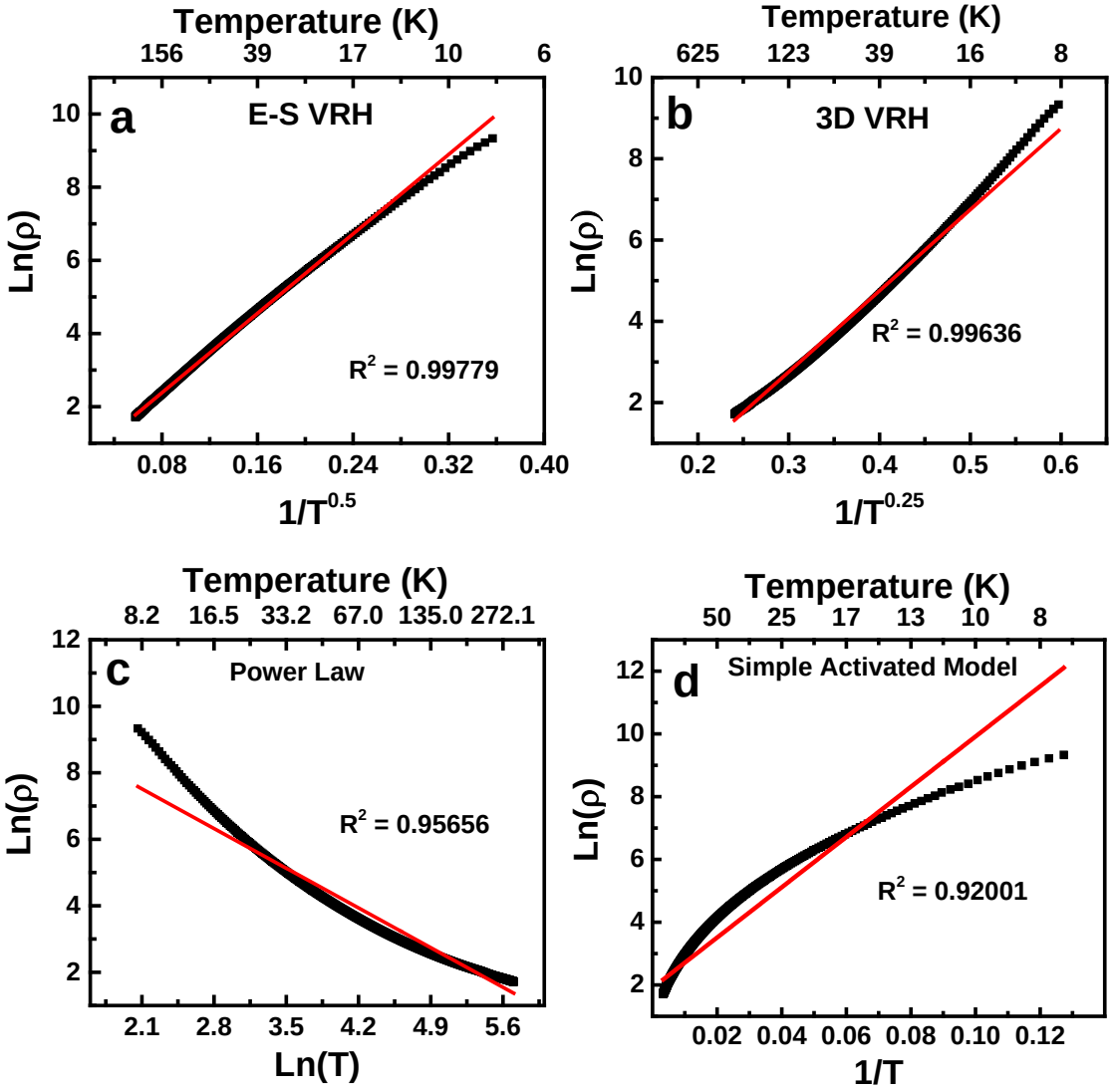

Figure S5. Fitting of the resistivity of a 22 µm thick *d*-$Nb_{1.33}CT_x$ film in the 7 to 300 K temperature range assuming: (a) E-S variable range hopping, (b) 3D variable range hopping (3D VRH), (c) power law and, (d) simple activated models.

References

1. Naguib, M.; Halim, J.; Lu, J.; Cook, K. M.; Hultman, L.; Gogotsi, Y.; Barsoum, M. W., New Two-Dimensional Niobium and Vanadium Carbides as Promising Materials for Li-ion Batteries. *J. Am. Chem. Soc.* **2013,** *135*, 15966-9.
2. Rietveld, H. M., A Profile Refinement Method for Nuclear and Magnetic Structures. *J. Appl. Crystallogr.* **1969,** *2*, 65-71.
3. Rodríguez-Carvajal, J., Recent Advances in Magnetic Structure Determination by Neutron Powder Diffraction. *Physica B: Condensed Matter* **1993,** *192*, 55-69.
4. Halim, J.; Kota, S.; Lukatskaya, M. R.; Naguib, M.; Zhao, M. Q.; Moon, E. J.; Pitock, J.; Nanda, J.; May, S. J.; Gogotsi, Y., Synthesis and characterization of 2D molybdenum carbide (MXene). *Adv. Funct. Mater.* **2016,** *26*, 3118-3127.

5. Halim, J.; Cook, K. M.; Naguib, M.; Eklund, P.; Gogotsi, Y.; Rosen, J.; Barsoum, M. W., X-Ray Photoelectron Spectroscopy of Select Multi-Layered Transition Metal Carbides (MXenes). *Appl. Surf. Sci.* **2016,** *362*, 406-417.
6. Halim, J., An X-Ray Photoelectron Spectroscopy Study of Multilayered Transition Metal Carbides (MXenes). Drexel University, **2016**.
7. Ghidiu, M.; Halim, J.; Kota, S.; Bish, D.; Gogotsi, Y.; Barsoum, M. W., Ion-Exchange and Cation Solvation Reactions in Ti_3C_2 MXene. *Chem. Mater.* **2016,** *28*, 3507-3514.
8. Halbritter, J.; Darlinski, A., Angle Resolved XPS Studies of Oxides at Nb-, NbN-, NbC- and Nb_3Sn- Surfaces. *IEEE Trans. Magn.* **1987,** *23*, 1381-1384.
9. Marques, M. T.; Ferraria, A. M.; Correia, J. B.; Rego, A. M. B. d.; Vilar, R., XRD, XPS and SEM Characterisation of Cu–NbC Nanocomposite Produced by Mechanical Alloying. *Mater. Chem. Phys.* **2008,** *109*, 174-180.
10. Miller, C. F.; Simmons, G. W.; Wei, R. P., High Temperature Oxidation of Nb, NbC and Ni_3Nb and Oxygen Enhanced Crack Growth. *Scr. Mater.* **2000,** *42*, 227-232.
11. Weibin, Z.; Weidong, W.; Xueming, W.; Xinlu, C.; Dawei, Y.; Changle, S.; Liping, P.; Yuying, W.; Li, B., The Investigation of NbO_2 and Nb_2O_5 Electronic Structure by XPS, UPS and First Principles Methods. *Surf. Interface Anal.* **2013,** *45*, 1206-1210.
12. Luo, Y.; Wang, P.; Ma, L. P.; Cheng, H. M., Hydrogen Sorption Kinetics of MgH_2 Catalyzed with NbF_5. *J. Alloys Compd.* **2008,** *453*, 138-142.
13. Dacca, A.; Gemme, G.; Mattera, L.; Parodi, R., XPS Analysis of the Surface Composition of Niobium for Superconducting RF Cavities. *Appl. Surf. Sci.* **1998,** *126*, 219-230.
14. Jayaweera, P. M.; Quah, E. L.; Idriss, H., Photoreaction of Ethanol on TiO_2(110) Single-Crystal Surface. *J. Phys. Chem. C* **2007,** *111*, 1764-1769.
15. Romero, R.; Ramos-Barrado, J. R.; Martin, F.; Leinen, D., Nb_2O_5 Thin Films Obtained by Chemical Spray Pyrolysis. *Surf. Interface Anal.* **2004,** *36*, 888-891.
16. Chen, L.; Sun, Q. Q.; Gu, J. J.; Xu, Y.; Ding, S. J.; Zhang, D. W., Bipolar Resistive Switching Characteristics of Atomic Layer Deposited Nb_2O_5 Thin Films for Nonvolatile Memory Application. *Current Applied Physics* **2011,** *11*, 849-852.
17. Guo, S. Q.; Zhang, X.; Zhou, Z.; Gao, G. D.; Liu, L., Facile Preparation of Hierarchical Nb_2O_5 Microspheres with Photocatalytic Activities and Electrochemical Properties. *Journal of Materials Chemistry A* **2014,** *2*, 9236-9243.
18. Beamson, G.; Briggs, D., *High Resolution XPS of Organic Polymers: The Scienta ESCA300 Database*. Wiley: **1992**.
19. Gulina, L.; Tolstoy, V.; Kasatkin, I.; Murin, I., Facile Synthesis of Scandium Fluoride Oriented Single-Crystalline Rods and Urchin-like Structures by a Gas–Solution Interface Technique. *CrystEngComm* **2017,** *19*, 5412-5416.
20. Nakayama, M.; Fukuda, M.; Konishi, S.; Tonosaki, T., Effects of Reaction Parameters on the Electrochemical Formation of Multilayer Films Composed of Manganese Oxides and Tetra-alkylammonium Ions. *J. Mater. Res.* **2006,** *21*, 3152-3160.